Developmental Biology 355 (2011) 32–42

Contents lists available at ScienceDirect

Developmental Biology

journal homepage: www.elsevier.com/developmentalbiology

The mechanism of lens placode formation: A case of matrix-mediated morphogenesis

Jie Huang [a], Ramya Rajagopal [a], Ying Liu [a], Lisa K. Dattilo [a], Ohad Shaham [b], Ruth Ashery-Padan [b], David C. Beebe [a,c,*]

[a] Department of Ophthalmology and Visual Sciences, Washington University School of Medicine, Saint Louis, MO, USA
[b] Sackler Faculty of Medicine, Department of Human Molecular Genetics and Biochemistry, Tel Aviv University, Tel Aviv, Israel
[c] Department of Cell Biology and Physiology, Washington University School of Medicine, Saint Louis, MO, USA

ARTICLE INFO

Article history:
Received for publication 19 October 2010
Revised 30 March 2011
Accepted 13 April 2011
Available online 21 April 2011

Keywords:
Placode formation
Extracellular matrix
Lens induction
Invagination

ABSTRACT

Although placodes are ubiquitous precursors of tissue invagination, the mechanism of placode formation has not been established and the requirement of placode formation for subsequent invagination has not been tested. Earlier measurements in chicken embryos supported the view that lens placode formation occurs because the extracellular matrix (ECM) between the optic vesicle and the surface ectoderm prevents the prospective lens cells from spreading. Continued cell proliferation within this restricted area was proposed to cause cell crowding, leading to cell elongation (placode formation). This view suggested that continued cell proliferation and adhesion to the ECM between the optic vesicle and the surface ectoderm was sufficient to explain lens placode formation. To test the predictions of this "restricted expansion hypothesis," we first confirmed that the cellular events that accompany lens placode formation in chicken embryos also occur in mouse embryos. We then showed that the failure of lens placode formation when the transcription factor, *Pax6* was conditionally deleted in the surface ectoderm was associated with greatly diminished accumulation of ECM between the optic vesicle and ectoderm and reduced levels of transcripts encoding components of the ECM. In accord with the "restricted expansion hypothesis," the Pax6-deleted ectoderm expanded, rather than being constrained to a constant area. As a further test, we disrupted the ECM by deleting *Fn1*, which is required for matrix assembly and cell–matrix adhesion. As in $Pax6^{CKO}$ embryos, the $Fn1^{CKO}$ lens ectoderm expanded, rather than being constrained to a fixed area and the lens placode did not form. Ectoderm cells in $Fn1^{CKO}$ embryos expressed markers of lens induction and reorganized their cytoskeleton as in wild type ectoderm, but did not invaginate, suggesting that placode formation establishes the minimal mechanical requirements for invagination.

Introduction

The formation of epithelial placodes is a recurring theme in morphogenesis. Placode formation is the first step in the formation of many ectodermally-derived structures, including the vertebrate central nervous system and sensory ganglia, ectodermal appendages, like hairs, scales and feathers, mammary glands, the insect tracheal system and salivary glands, the eye lens, the inner ear and many others. Soon after their formation, most placodes invaginate, transforming surface epithelia into internal structures. Most research has focused on this second stage of placode morphogenesis, invagination, while the mechanisms leading to placode formation have only rarely been explored (Zwaan and Hendrix, 1973). It seems possible that placode formation is an essential precondition for invagination, but the requirement of placode formation for subsequent epithelial morphogenesis has not been tested.

Lens formation from head ectoderm and the transformation of the optic vesicle into the optic cup are the major morphogenetic events of eye formation. In mouse embryos, the morphogenesis of the eye commences on embryonic day 9 (E9), when the neural epithelium of the ventral forebrain evaginates to form the bilateral optic vesicles. The optic vesicles soon contact and adhere to the head surface ectoderm on each side of the embryo (Fig. 1A). Where contact occurs and in a small region ventral to the optic vesicle, the surface ectoderm thickens, forming the lens placodes (Fig. 1B). After a lens placode forms, it and the prospective retina invaginate, giving rise to the lens pit and optic cup. The lens pit subsequently separates from the surface ectoderm to form the lens vesicle, which differentiates into the lens. The optic cup differentiates into the retina, ciliary epithelia, iris epithelia and the retinal pigment epithelium.

The cellular processes associated with the formation of the lens placode were studied most extensively in chicken embryos more than 30 years ago. Placode formation involves the transformation of the prospective lens ectoderm cells from a cuboidal to columnar shape; the cells do not multilayer (Zwaan and Hendrix, 1973). At the time of lens placode thickening, cell density increases in the placodal

* Corresponding author at: Dept. Ophthalmology and Visual Sciences, Washington University School of Medicine, Saint Louis, MO 63110, USA. Fax: +1 314 747 1405.
E-mail address: beebe@wustl.edu (D.C. Beebe).

0012-1606/$ – see front matter © 2011 Elsevier Inc. All rights reserved.
doi:10.1016/j.ydbio.2011.04.008

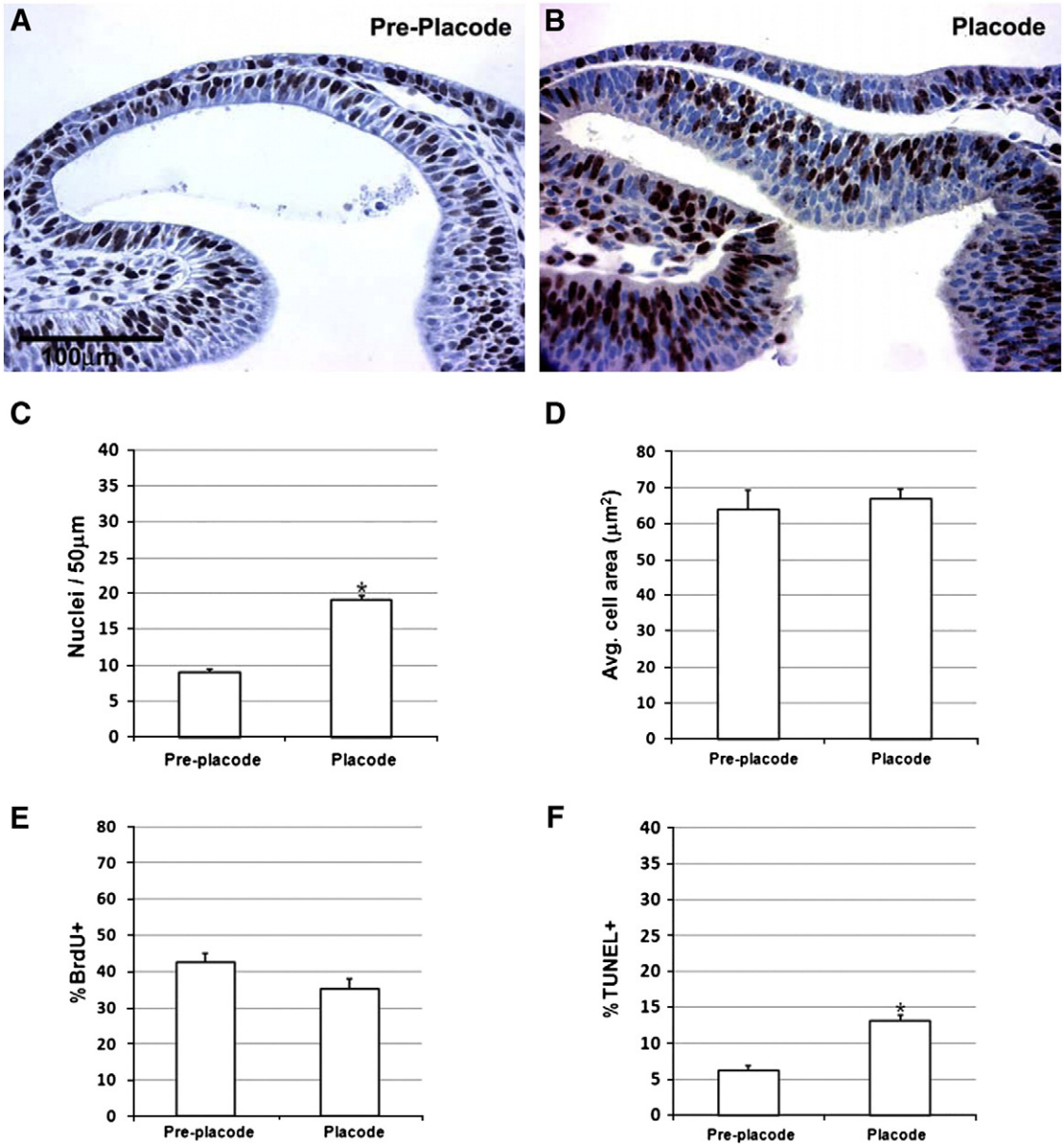

Fig. 1. Cell density, area, proliferation and death in wild type mouse embryos during lens placode formation. Measurements were made at the pre-placode stage (A) and at placode stage (B). Embryos in A and B were BrdU-labeled. Cell density (number of nuclei/50 µm length) doubled during placode formation (C). Cell area (nuclei per tissue area; D) and cell proliferation (BrdU labeling index; E) did not change during placode formation. Cell death increased during placode formation (F). *$p<0.05$.

ectoderm (McKeehan, 1951; Zwaan and Hendrix, 1973). The mitotic index and the tritiated thymidine labeling index within and outside the forming placode are similar and average cell area remains constant, indicating that the placodal ectoderm does not thicken due to a local increase in cell proliferation or volume (McKeehan, 1951; Zwaan and Pearce, 1971). Zwaan and co-workers noted that that an abundant extracellular matrix was deposited between the surface ectoderm and optic vesicle after their contact and the area of contact between these tissues remained constant during placode formation (Hendrix and Zwaan, 1974, 1975; Zwaan and Webster, 1984). Based on these observations, they hypothesized that adhesion between the optic vesicle and the overlying ectoderm, mediated by the extracellular matrix, prevented the expansion of the lens territory (Zwaan and Hendrix, 1973). With continued cell proliferation, this led to cell crowding, cell elongation and placode formation. We refer to this as the "restricted expansion hypothesis" of lens placode formation. This hypothesis predicts that, as long as cell proliferation continues, adhesion of the ectoderm cells to the underlying matrix is sufficient to explain lens placode formation.

In the present study, we analyzed lens placode formation in wild type mouse embryos, which confirmed that similar events occur during lens placode formation in birds and mammals. We then tested the predictions of the "restricted expansion hypothesis" in embryos in which lens placode formation was prevented by conditional deletion of the transcription factor, *Pax6*, from the ectoderm and in embryos in which the assembly of the ECM was disrupted by global deletion of *Fn1*.

Materials and methods

Genotyping and tamoxifen injection

All animals were treated in accordance with the ARVO Statement for the Use of Animals in Ophthalmic and Vision Research and with

the approval of the Animal Studies Committee of the Washington University School of Medicine. Mice expressing Cre recombinase in the surface ectoderm (*Le-Cre*), or optic vesicle (*Rx-Cre*) and tamoxifen-inducible Cre (*CAGG-Cre^{ERTM}*) were described previously (Ashery-Padan et al., 2000; Hayashi and McMahon, 2002; Swindell et al., 2006). *Fn1$^{fx/fx}$* mice were reported in previous studies (Sakai et al., 2001). Noon of the day when the vaginal plug was detected was considered embryonic day (E) 0.5 of development. Embryos were also staged by counting somite pairs at the time of collection. Early placode formation was considered to occur at 20–24 somites and late placode at 28–34 somites (Garcia et al., 2011). For animals carrying the Le-Cre transgene, matings between mice that were homozygous for the floxed allele in which the female was also Cre-positive, resulted in litters in which about half of the offspring were Cre-positive (conditional knockout; CKO), the others were Cre-negative (wild type; WT). For tamoxifen-inducible Cre, matings were between the *Fn1$^{fx/+}$*, *CAGG-Cre^{ERTM}* and *Fn1$^{fx/fx}$* mice. The *Fn1$^{fx/+}$*, *CAGG-Cre^{ERTM}* was the control for potential tamoxifen toxicity, as described previously (Naiche and Papaioannou, 2007). Doses of 6 mg 4-OH tamoxifen dissolved in corn oil were injected intraperitoneally into pregnant dams at E8.5 and E8.75. Embryos were collected at the desired stages ($n=3$ to 5 for each genotype and stage).

Histology

Embryo heads were fixed in 4% paraformaldehyde/PBS overnight at 4 °C, dehydrated through a series of ethanol concentrations, embedded in paraffin and sectioned at 4 μm. For morphological studies, sections were stained with hematoxylin and eosin (Surgipath, Richmond, IL, USA). Measurements of cell area, cell proliferation, cell length, and apoptosis were performed on a minimum of three sections from five eyes. Cell area was determined by dividing the average cell area (μm^2) by the number of nuclei from sections of E9.5 embryo heads using the Spot camera software (Spot Diagnostic Instruments, Sterling Heights, MI). Since average cell area is proportional to average cell volume, lack of change in cell area indicates no change in cell volume (Gundersen et al., 1988). Cell density was determined by counting the number of nuclei per 50 μm length of the ectoderm. To analyze the thickness of the placode, 5 equidistant points were marked along the length of the placode and the height of the tissue was measured at those points. The ventral-most region of the lens placode is not in contact with the optic vesicle, even though it contributes to the lens vesicle (see Fig. 5E). This region was included in these measurements. The extent of contact between the surface ectoderm and the optic vesicle was measured in serial sections through the area of contact.

TUNEL, EdU and BrdU labeling

Terminal deoxynucleotidyl transferase (TdT)-mediated deoxyuridine triphosphate nick end-labeling (TUNEL) was done with an Apoptag kit (Chemicon, Temecula, CA). The deparaffinized slides were treated with 3% H_2O_2 in methanol for 30 min, followed by proteinase K treatment (20 μg/ml) for 15 min. Slides were incubated with TdT enzyme in equilibration buffer for 1 h at 37 °C. The reaction was terminated with wash buffer provided by the manufacturer for 10 min at RT and then incubated with anti-digoxigenin-peroxidase conjugate for 30 min at RT, followed by DAB + H_20_2 treatment. Slides were counterstained with hematoxylin.

For BrdU staining, pregnant females were injected with 50 mg/kg of body weight of 10 mM BrdU (Roche, Indianapolis, IN) and 1 mM 5-fluoro-5′-deoxyuridine (Sigma, St. Louis, MO) and sacrificed after 1 h. A monoclonal anti-BrdU antibody (1:250) (Dako, Carpinteria, CA) was used with a Vectastain Elite Mouse IgG ABC kit as described above. Sections were counterstained with hematoxylin.

For EdU staining, pregnant females were injected intraperitoneally with 100 μg of 5-ethynyl-2′-deoxyuridine (EdU) (Invitrogen, Carlsbad, CA) 1 h prior to death. Embryos were fixed and sectioned as above. EdU was detected with AlexaFluor 488-azide using a Click-iT™ Kit for 1 h according to manufacturer's instructions (Invitrogen). Total nuclei were counterstained with DRAQ-5 (1:1000; Biostatus Limited, Shepshed, Leicestershire, UK) for 30 min at RT in 1X PBS. Sections were rinsed in 1X PBS and viewed using a Zeiss 510 confocal microscope (Carl Zeiss Microimaging, Inc., Thornwood, NY,).

Immunohistochemical staining on paraffin sections

Embryos were fixed as described above, embedded in 5% agarose, processed and embedded in paraffin, sectioned at 4 μm, deparaffinized and rehydrated. Endogenous peroxidase activity was inactivated with 3% H_2O_2 in methanol for 30 min at RT for those samples that would be treated for horseradish peroxidase (HRP). Epitope retrieval was performed in 0.01 M citrate buffer (pH 6.0) by placing the slides in a pressure cooker for 3 min. Slides were then incubated in blocking solution containing 20% inactivated normal donkey serum for 30 min at RT followed by incubation in primary antibodies overnight at 4 °C. Slides were then incubated for 1 h at RT either with Alexa-Fluor-labeled secondary antibodies (Molecular Probes, Eugene, OR) or biotinylated secondary antibodies (Vector Laboratories, Burlingame, CA). Slides incubated with biotinylated secondary antibodies were treated with the ABC-peroxidase reagent from Vectastain Elite ABC Kit (Vector Laboratories, Burlingame, CA) followed by treatment with diaminobenzidine (DAB) (Sigma, St. Louis, MO) and H_20_2, washed with PBS and counterstained with hematoxylin (Surgipath, Richmond, IL).

Immunofluorescent staining on thick sections

Embryos were fixed as described above. After rinsing in PBS, heads were dissected in half, embedded in 4% agarose in PBS and allowed to set overnight at 4 °C. Thick sections (120 μm) were cut using a tissue slicer (Electron Microscopy Sciences, Hatfield, PA). Sections containing the lens placodes were blocked in 5% normal goat serum, 0.5% Triton-X 100 for permeabilization, and 0.03% sodium azide for 1 h at RT and incubated with primary antibodies overnight at 4 °C. After rinsing, sections were incubated with fluorescent labeled secondary antibodies for 1 h at RT and counterstained with DRAQ-5 (1:1000; Biostatus Limited, Shepshed, Leicestershire, UK), a vital, fluorescent DNA dye. Sections were mounted in Vectashield (Vector Laboratories, Burlingame, CA).

In situ hybridization on frozen sections

Frozen sections were fixed in 4% paraformaldehyde/PBS, treated with proteinase K (10 μg/ml), post-fixed in 4% paraformaldehyde/PBS and acetylated in triethanolamine-acetic anhydride solution. Samples were pre-hybridized in 50% formamide, 5 × SSC, 5 mM EDTA, 1 × Denhardt's, 100 ug/ml heparin, 0.3 mg/ml yeast tRNA and 0.1% Tween-20, incubated in the same solution with riboprobes overnight, washed with 0.2 × SSC, blocked in 10% lamb serum and incubated with anti-digoxigenin antibody overnight. The color reaction was developed using NBT and BCIP in the dark. After the reaction was completed, the slides were washed in PBS, fixed in 4% paraformaldehyde/PBS and mounted in 100% glycerol. Digoxigenin-labeled riboprobes were synthesized from cDNA generated from RNA isolated from wild-type E9.5 embryos using the following PCR primer pairs:

Fn1: 5′-gatcggcagggagaaaatgg-3′; 5′-tggggtgtggattgaccttg-3′
Vcan: 5′-ctggcacaaattccaaggacag-3′; 5′-cgctgaatgaaaccatctttgc-3′
Tnc: 5′-ggcagatatggggacaataacc-3′; 5′-gcaaggggtaacttccaatgac-3′

Antibodies

The primary antibodies used were to phospho-histone H3 (1:1000; Upstate Biotechnology, Lake Placid, NY), cleaved caspase3 (1:200; Cell Signaling Technology, Danvers, MA), Pax6 (1:500; Developmental Studies Hybridoma Bank, Iowa City, IA), fibronectin (1:250; Millipore Corp., Billerica, MA) and Sox2 (1:500; Cell Signaling Technology).

PAS and Alcian Blue staining

For Periodic Acid Schiff (PAS) staining, sections were deparaffinized, hydrated to water, oxidized in periodic acid for 5 min, treated with Schiff's reagent for 15 min, washed and counterstained with hematoxylin using the Accustain PAS kit (Sigma, St. Louis, MO). For Alcian Blue staining, sections were deparaffinized, hydrated to water, and stained in Alcian Blue for 30 min.

Imaging

All the brightfield images were taken using an Olympus BX60 microscope (Olympus, Melville, NY) and Spot camera (Spot Diagnostic Instruments, Sterling Heights, MI). The fluorescent images were taken either using a Olympus BX51 with Spot camera or a Zeiss 510 confocal microscope (Carl Zeiss, Thornburgh, NY).

Laser microdissection and microarray analysis

E9.5 embryos were embedded in OCT and snap frozen on dry ice for 10–15 min. 10 μm frozen sections were transferred to glass PEN foil slides (Leica Microsystems, #11505189). To avoid the separation of the foil and slides, slides were dipped in 70% ethanol at 4 °C for 1 min, washed in RNAase-free water twice for 30 s, rinsed in 95% ethanol, and stained in Eosin Y. Stained samples were washed in 95% ethanol and dehydrated in 100% ethanol and xylene. The slides were dried and the lens placode or prospective lens ectoderm was microdissected using a Leica LMD 6000 laser microdissection system. Approximately 50 ng of total RNA was extracted from the tissue obtained from one embryo using a Qiagen RNeasy Microkit (Qiagen#74004). 15 ng of total RNA was amplified to produce 3–5 μg of cDNA using Nugen WT-Ovation™ Pico RNA Amplification System (NuGEN Technologies Inc, #3300-12). Triplicate cDNA samples were used to probe Illumina Mouse6 bead microarrays. Microarray data were analyzed using Illumina Genome Studio software. The data in Table 1 are derived from expression data from 18 arrays of wild type E9.5 placodes compared to data from 9 arrays probed with cDNA from *Pax6*^{CKO} ectoderm.

Table 1
Transcripts significantly altered in E9.5 *Pax6*^{CKO} embryos, as determined by microarray analysis. Results from eighteen microarrays from wild type and nine from *Pax6*^{CKO} ectoderm are summarized by these data.

Category	Gene	Fold change	p-value
Transcription factors known to be regulated by Pax6 and/or important for lens development	*c-Maf*	−12	<0.001
	Prox1	−8	<0.001
	Mab21l1	−2.5	<0.001
	Tcfap2a	−1.8	<0.01
	Pitx3	−46	<0.01
	Sox2	−2.2	<0.001
Expressed by the LeCre transgene	*eGFP*	91	<0.001
Extracellular matrix and related transcripts	*Fn1*	−3.7	<0.001
	Vcan	−2.3	<0.001
	Leprel1 (P3h2)	−4.5	<0.001
	Has2	−3.2	<0.001
	Tnc	−10.3	<0.001
	Tgm2	−13.0	<0.001
	Col13a1	−12.0	<0.001

Explant culture

Pregnant dams were injected i.p. with 180 mg/kg 4-OH tamoxifen at E8.5 and E9.25 and the embryos were collected at E9.75. Heads were dissected into halves; one half was cultured in medium supplemented with 10 μM 4-OH tamoxifen and the other in medium with vehicle (ethanol). Heads were cultured on a Micropore filter (Costar, #110414) floating on Dulbecco's Modified Eagle's Medium (DMEM) supplemented with 20% fetal bovine serum, 100 μM non-essential amino acids, 100 units penicillin and 100 μg/ml streptomycin. Tissues were harvested at E11.5, fixed for 30 min and then used for immunostaining or in situ hybridization.

Statistical tests

Unpaired Student's *t*-test was performed using GraphPad InStat, Version 3.05.

Results

Comparison of lens placode formation in the mouse and chick

Previous studies showed that lens placode thickening in chicken embryos is accompanied by an increase in cell density, but the mitotic index, thymidine labeling index, and cell volume of the placode cells did not differ from the adjacent, non-placodal tissue (McKeehan, 1951; Zwaan and Pearce, 1971). We determined whether the same was true during mouse lens placode formation (Figs. 1A, B). We found that the cell density was twice as high in the lens placode as in the pre-placodal ectoderm of mouse embryos (Fig. 1C). However, the average area per cell in tissue sections was not different in the pre-placode and placode, indicating that average cell volume remained constant during placode formation (Fig. 1D). To determine if the cell crowding that accompanies placode formation is driven by increased proliferation or decreased cell death, we performed BrdU-labeling and TUNEL assays before and during placode formation. The percentage of BrdU-labeled nuclei was indistinguishable in the pre-placode ectoderm at E8.5 and the placode at E9.5 (Fig. 1E). The BrdU labeling index was also similar in the placodal and peri-placodal ectoderm at E9.5 (Supplemental Fig. S1). Instead of a decrease in cell death, which could increase cell density, we found a greater than 2-fold increase in the TUNEL labeling index in the lens placode compared to the pre-placode ectoderm (Fig. 1F), an observation confirmed using an antibody against activated caspase-3 (data not shown). Similarly, cell death was more than twice as high in the lens placode as in the adjacent periplacodal ectoderm by TUNEL assay or antibody to activated caspase-3 (Supplemental Fig. S1).

Pax6 is required for lens placode formation and to restrain spreading of the ectoderm

Conditional deletion of the transcription factor, *Pax6*, demonstrated that it is required in the surface ectoderm for lens formation (Ashery-Padan et al., 2000; Smith et al., 2009). Because the extent of placode thickening was not measured in these studies, we determined the thickness of the surface ectoderm in *Pax6*$^{+/+;\ LeCre\pm}$ (wild type; *WT*), *Pax6*$^{+/fx;\ LeCre+}$ (lens ectoderm-specific *Pax6* heterozygote) and *Pax6*$^{fx/fx;\ LeCre+}$ (lens ectoderm-specific *Pax6* conditional knockout; *CKO*) embryos (Figs. 2A–C). At the lens placode stage, the *Pax6*^{CKO} surface ectoderm was significantly thinner than wild type (Fig. 2D) and indistinguishable from the pre-placodal ectoderm at E8.5 (data not shown). Ectoderm-specific heterozygosity for *Pax6* produced placodes of intermediate thickness, consistent with the haploinsufficiency seen in mice and humans heterozygous for *Pax6* (Fig. 2D). Cell area, proliferation and apoptosis were not different in the *Pax6*^{CKO} surface ectoderm before lens placode formation and at the time lens

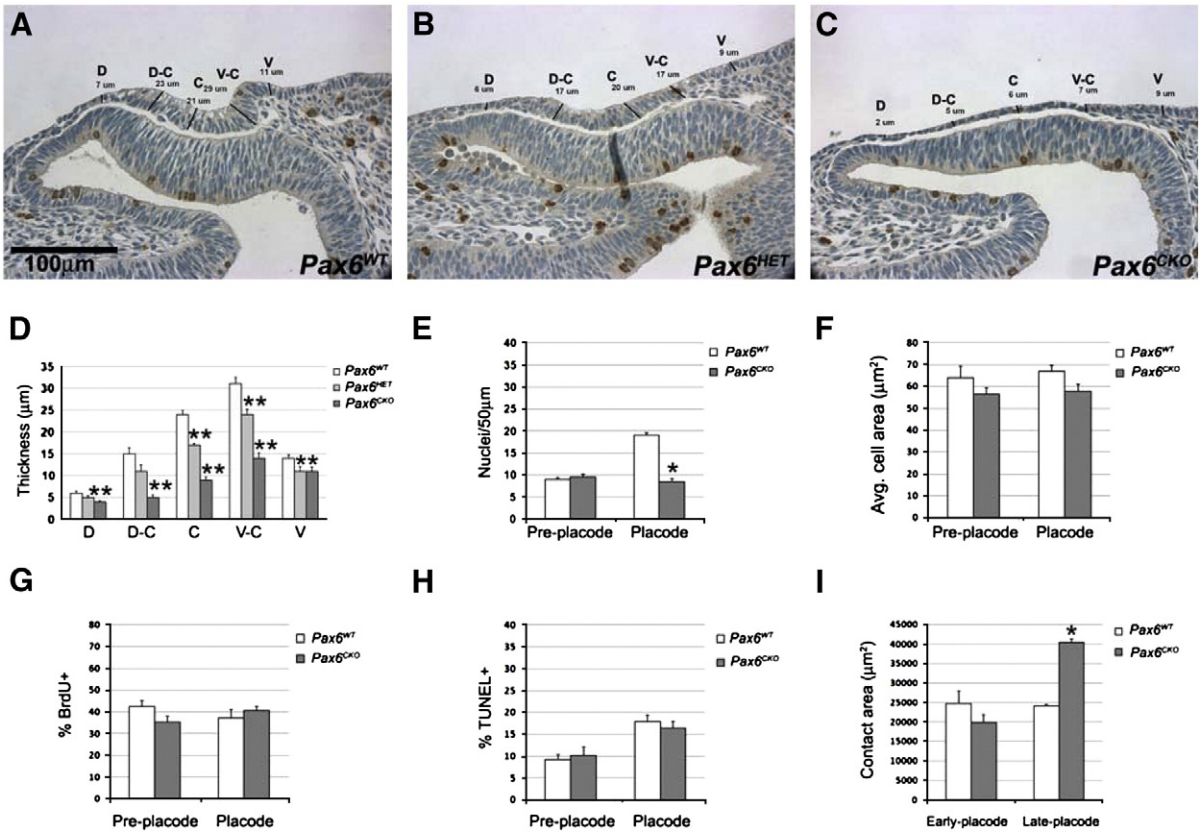

Fig. 2. Placode thickness is regulated by *Pax6* dose and correlates with cell density. (A) Placode thickness of wild type ($Pax6^{+/+}$), (B) ectoderm-specific conditional heterozygote ($Pax6^{HET}$) and (C) ectoderm-specific conditional knockout ($Pax6^{CKO}$) embryos was measured at five positions: dorsal (D), dorsal-center (D-C), center (C), ventral-center (V-C) and ventral (V). (D) $Pax6^{CKO}$ ectoderm was significantly thinner than wild type at all locations; heterozygous placodes were of intermediate thickness. (E) Unlike wild type ectoderm, average cell density did not increase in $Pax6^{CKO}$ ectoderm. (G) Average cell area, (F) cell proliferation (BrdU labeling index) and (H) cell death (TUNEL labeling index) were not significantly different in $Pax6^{+/+}$ and $Pax6^{CKO}$ embryos at pre-placode and placode stages. (I) contact area between the optic vesicle and the ectoderm was unchanged during lens placode formation in wild type embryos, but increased in $Pax6^{CKO}$ littermate embryos. *$p<0.05$, ** $p<0.01$.

placode should have formed. However, cell density was lower in the $Pax6^{CKO}$ surface ectoderm compared to $Pax6^{WT}$ (Figs. 2E–H). In agreement with measurements in chicken embryos, the contact area between the optic vesicle and the surface ectoderm remained constant during placode formation in wild type embryos (Fig. 2I). However, the contact area between these tissues increased in $Pax6^{CKO}$ embryos, indicating that the ectoderm spread, rather than being constrained to a constant area.

Placodal Pax6 regulates the expression and deposition of components of the ECM

We used microarray analysis to identify genes that are regulated by Pax6 in the lens placode. In three separate studies, triplicate samples of wild type and $Pax6^{CKO}$ surface ectoderm were collected at E9.5 by laser microdissection (Supplemental Figs. S2A, B) and RNA was isolated and amplified for microarray analysis. When the data from all three microarray studies were combined, 772 transcripts were significantly decreased and 512 significantly increased in the $Pax6^{CKO}$ placodes. Among the transcripts that were decreased were well-known Pax6 targets and transcription factors required for normal lens development, including *Prox1*, *Sox2*, *Mab21l*, *Pitx3*, *Tcfap2a* and *Maf* (Table 1) (Ashery-Padan et al., 2000; Cvekl and Duncan, 2007; Lang, 2004; Reza et al., 2002; Smith et al., 2009). Several transcripts encoding components of the extracellular matrix (ECM) or involved in assembly of the ECM, such as fibronectin1 (*Fn1*), versican (*Vcan*), tenascin-C (*Tnc*), hyaluronan synthase 2 (*Has2*), leprecan-like 1 (*Leprel1*; prolyl 3-hydroxylase 2), and the α1 chain of collagen type 13 (*Col13a1*) were significantly decreased in the $Pax6^{CKO}$ placodes (Table 1). In situ hybridization confirmed that transcripts encoding *Fn1*, *Vcan* and *Tnc* were decreased in the $Pax6^{CKO}$ surface ectoderm (Supplemental Figs. 2C–H). PAS and Alcian blue staining showed markedly decreased ECM in $Pax6^{CKO}$ embryos, compared to *WT* (Figs. 3A–D), demonstrating that Pax6 in the surface ectoderm is required for the accumulation of the ECM between the surface ectoderm and optic vesicle and that the lens placode is a major source of this ECM.

Deletion of Fn1 permitted the ectoderm to spread and prevented placode formation

To test the function of ECM in lens placode formation, we conditionally deleted *Fn1*. Fibronectin contains modules that bind to a variety of extracellular and cell surface molecules, including collagens, glycosaminoglycans, fibrin, integrins and fibronectin itself, and is crucial for ECM assembly and for mediating adhesion between cells and their ECM (Akiyama et al., 1989; Corbett et al., 1997; Huang et al., 2007; Leiss et al., 2008; Mattey and Garrod, 1984; Oberley and Steinert, 1983; Wierzbicka-Patynowski and Schwarzbauer, 2003). Because the *Fn1* germline knockout is lethal (George et al., 1993), we conditionally deleted *Fn1* from surface ectoderm, optic vesicle, or both using *Le-Cre*, *Rx-Cre* or both transgenes (Ashery-Padan et al., 2000; Swindell et al., 2006). None of these prevented placode formation or lens invagination (Supplemental Figs. S3A–D). However, in each case, residual Fn1 was present between the lens placode and optic vesicle, suggesting that deletion did not occur completely or early enough to deplete fibronectin from the ECM, or that fibronectin was produced by the adjacent periocular mesenchyme cells.

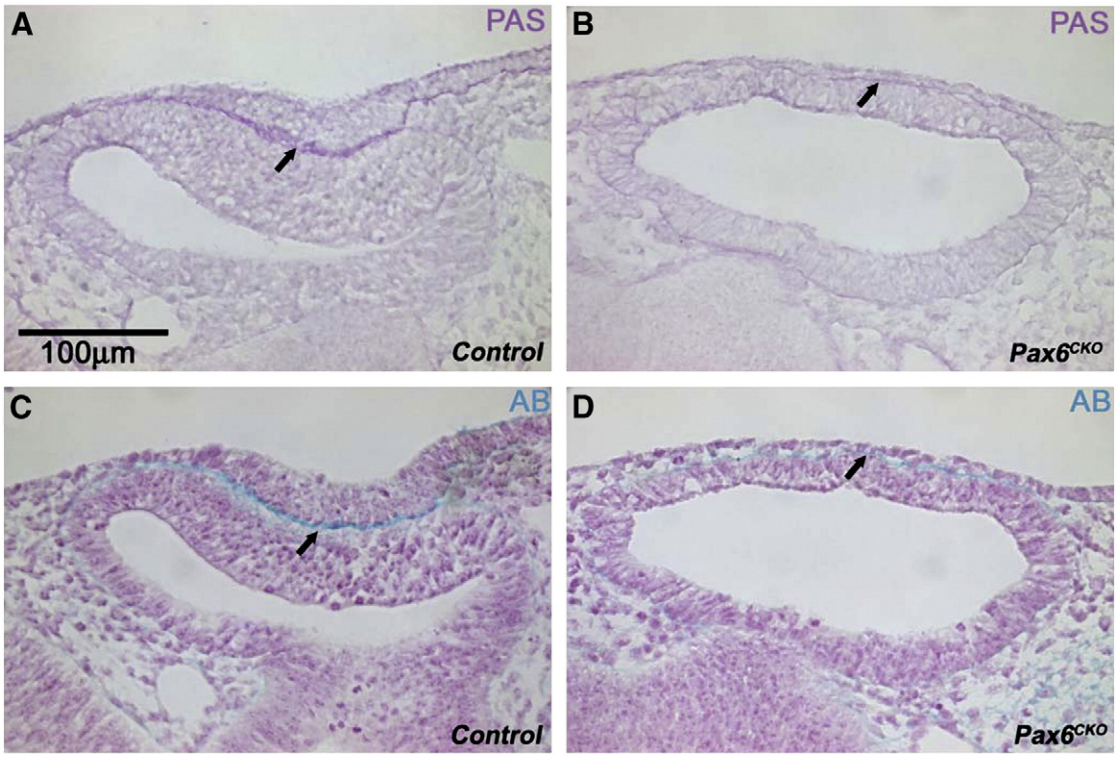

Fig. 3. The matrix between the optic vesicle and the ectoderm is diminished in *Pax6*^{CKO} embryos. Periodic acid-Schiff (PAS) and Alcian Blue (AB) staining in *Pax6*^{WT} and *Pax6*^{CKO} littermate embryos. Staining of the matrix between the optic vesicle and the surface ectoderm (arrows) was intense in *Pax6*^{WT}, but decreased markedly in *Pax6*^{CKO} embryos. Staining of the matrix posterior to the optic vesicle was similar in wild type and knockout embryos.

To address these possibilities we deleted *Fn1* globally and at an earlier stage by administering tamoxifen at E8.5 and E8.75 to pregnant dams with embryos that were *Fn1*$^{fx/+}$ or *Fn1*$^{fx/fx}$ and carried the *CAGG-Cre*^{ERTM} transgene (Hayashi and McMahon, 2002). We also introduced the *Le-Cre* transgene into this cross, since this construct expresses green fluorescent protein (GFP) from an internal ribosome entry site, thereby marking the prospective lens-forming ectoderm (Ashery-Padan et al., 2000).

Global deletion of *Fn1* prevented lens placode formation and invagination. Distinct GFP fluorescence demarcated the lens pit cells in *CAGG-Cre*^{ERTM}; *Fn1*$^{fx/+}$ embryos at E10.5, but fluorescence was weaker and more broadly distributed in tamoxifen-treated *CAGG-Cre*^{ERTM}; *Fn1*$^{fx/fx}$ embryos (insets in Figs. 4A, B). At E10.5, *CAGG-Cre*^{ERTM}; *Fn1*$^{fx/fx}$ embryos had not formed a lens placode, while the *CAGG-Cre*^{ERTM}; *Fn1*$^{fx/+}$ littermates had an invaginating lens vesicle (Figs. 4C, D). Staining for fibronectin in *CAGG-Cre*^{ERTM}; *Fn1*$^{fx/fx}$ embryos showed that the earlier and more extensive deletion greatly decreased the amount of fibronectin beneath ectoderm, resulting in sparse, discontinuous fibronectin staining in the extracellular matrix (Fig. 4D).

Global deletion of *Fn1* resulted in pericardial edema at E10.5 (Figs. 4A, B) and most of the *Fn1*^{CKO} embryos died before E11.0, which is consistent with the function of fibronectin in vascular development (George et al., 1993). To be sure that inhibition of lens placode formation resulted from the deficiency in *Fn1* and not from secondary effects, like the vascular defects seen in *Fn1*^{CKO} embryos, we cultured bisected heads beginning at E9.5, a day before the embryos developed pericardial edema. In this study, all pregnant dams received tamoxifen at E8.5 and E9.25. At E9.5, the embryos were removed and one half-head from each embryo was cultured in 4-OH tamoxifen and the other half was cultured with vehicle (ethanol). We then compared lens placode and vesicle formation in embryos that carried one floxed *Fn1* allele (*Fn1*$^{fx/+}$; control) to embryos in which both *Fn1* alleles were floxed (*Fn1*$^{fx/fx}$). Lens vesicles formed in the head explants from control *CAGG-Cre*^{ERTM}; *Fn1*$^{fx/+}$ embryos, whether they were cultured in supplemental tamoxifen or not (Figs. 4E, F, I, J). In heads of *CAGG-Cre*^{ERTM}; *Fn1*$^{fx/fx}$ embryos that were cultured without supplemental tamoxifen, no lens vesicles formed, although small aggregates of lens cells ("lentoids") were sometimes seen (Figs. 4G, H). When tamoxifen was present in the culture medium, lens vesicles or lentoids were not detected (Figs. 4K, L).

The thickness of the lens placode in *Fn1*-deficient head explants was significantly decreased compared to control *CAGG-Cre*^{ERTM}; *Fn1*$^{fx/+}$ head explants (Fig. 5A). As in the *Pax6*^{CKO} placodes, the contact area between the ectoderm and the optic vesicle expanded in *Fn1*-deficient explants, showing that the ectoderm spread, rather than being constrained by adhesion to the ECM (Fig. 5B).

Previous studies showed that the ECM can regulate cell growth and apoptosis (Almeida et al., 2000; Danen and Yamada, 2001; Oberley and Steinert, 1983). To determine if the failure of lens placode formation in *Fn1* deficient head explants was due to decreased proliferation or increased cell death, we performed EdU and TUNEL analyses. The percentage of cells in S-phase, as detected with EdU staining, was not significantly altered in *Fn1*-deficient head explants (Fig. 5C). Cell death increased two-fold in the *Fn1*-deficient embryos (Fig. 5D). However, in previous studies in which BMP or FGF receptors (*Bmpr1a* or *Fgfr2*) were deleted in the ectoderm, apoptosis was similar to or higher than in the *Fn1*^{CKO} ectoderm, but this level of apoptosis did not prevent the formation of the lens placode or its subsequent invagination (Garcia et al., 2011; Rajagopal et al., 2009).

Previous studies showed that the ECM might play a role in sequestering morphogens involved in inductive tissue interactions. For example, heparan sulfate proteoglycans serve as co-receptors for FGFs (Allen and Rapraeger, 2003; Pan et al., 2008; Smith et al., 2007) and BMPs interact with and accumulate in the ECM (Gregory et al., 2005; Seib et al., 2009; Zhu et al., 1999). If the ECM were disrupted, morphogens might diffuse more readily, reducing their concentration and, perhaps, their inductive ability. By deleting FGF receptors (*Fgfr1*

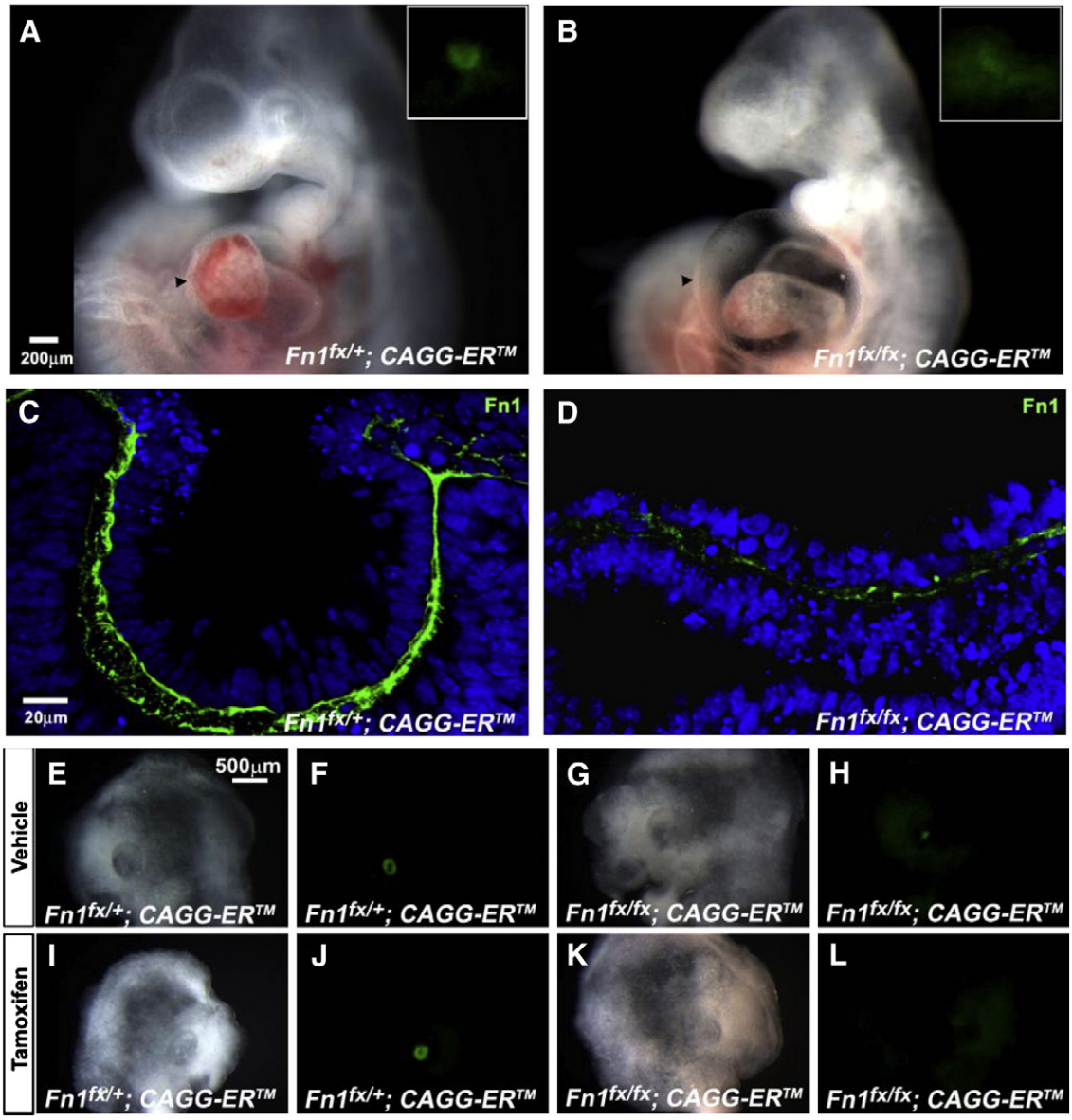

Fig. 4. Lens formation and immunostaining for fibronectin in *Fn1*-deficient embryos and cultured heads. (A) The lens vesicle formed in a $Fn1^{fx/+}$ embryo exposed to tamoxifen on E8. GFP fluorescence, which marks the prospective lens tissue, is strong and sharply demarcated (inset). (B) No lens vesicle formed in a $Fn1^{fx/fx}$ embryo exposed to tamoxifen. GFP fluorescence in the ectoderm was weak and diffuse (inset) and the embryo has pericardial edema (arrowhead). (C) Fibronectin immunostaining was robust in a $Fn1^{fx/+}$embryo exposed to two doses of tamoxifen on E8. (D) Fibronectin immunostaining decreased greatly and became discontinuous in $Fn1^{fx/fx}$ embryos exposed to two doses tamoxifen on E8. Lens formation in $Fn1^{fx/+}$ and $Fn1^{fx/fx}$ head explants from embryos exposed to tamoxifen at E8.5 and E9.25 and cultured with or without tamoxifen from E9.5 to E11.5 (E, F, I, J). Brightfield and fluorescence images showing that lens vesicles formed in $Fn^{+/fx}$; $CAGG\text{-}ER^{TM}$ head explants exposed to tamoxifen in E8 and cultured at E9.5 in vehicle (E, F) or in tamoxifen (I, J). (G, H) Brightfield and fluorescence images showing a small aggregate of lens cells ("lentoid"). Lentoids sometimes formed in $Fn^{fx/fx}$; $CAGG\text{-}ER^{TM}$ head explants that received no supplemental tamoxifen during culture. (K, L) Brightfield and fluorescence images showing that lens vesicles were absent from cultured heads of $Fn^{fx/fx}$; $CAGG\text{-}ER^{TM}$ embryos when tamoxifen was added to the culture medium.

and *Fgfr2*) in the prospective lens placode, we recently showed that FGF signaling is unlikely to be required for lens induction (Garcia et al., 2011). However, BMP4 is produced by the optic vesicle and BMP receptors are required in the ectoderm for lens formation (Furuta and Hogan, 1998; Rajagopal et al., 2009). To determine whether BMP signaling was impaired in the $Fn1^{CKO}$ embryos, we stained for BMP-activated Smads (phosphorylated Smad1/5/8) in the surface ectoderm. Nuclear staining for phosphorylated Smad1/5/8 was detected in the nuclei of heterozygous and *Fn1*-deficient ectoderm cells (Figs. 5E, F). Before lens induction, Pax6 levels are low in the prospective lens-forming ectoderm ($Pax6^{preplacode}$) and increase during induction ($Pax6^{placode}$) (Lang, 2004). Comparison of Pax6 levels in the ectoderm and distal optic vesicle of $Fn1^{+/fx}$ and $Fn1^{fx/fx}$ embryos that expressed tamoxifen-inducible Cre showed that Pax6 was not decreased in *Fn1*-deficient head explants (Figs. 5G, H), suggesting that lens induction by BMPs occurred normally.

The cytoskeletal reorganization that accompanies lens invagination occurs in the absence of placode formation

Although placode formation and invagination are distinct morphogenetic events, they have rarely been studied as separate processes. Therefore, it is not clear whether placode formation is required for subsequent invagination. Invagination of the lens placode involves the BMP-dependent re-localization of actin microfilaments from the periphery to the apical ends of the placode cells, accompanied by the apical localization of myosin II (Plageman et al., 2010; Rajagopal et al., 2009). These events are followed by constriction of the cell

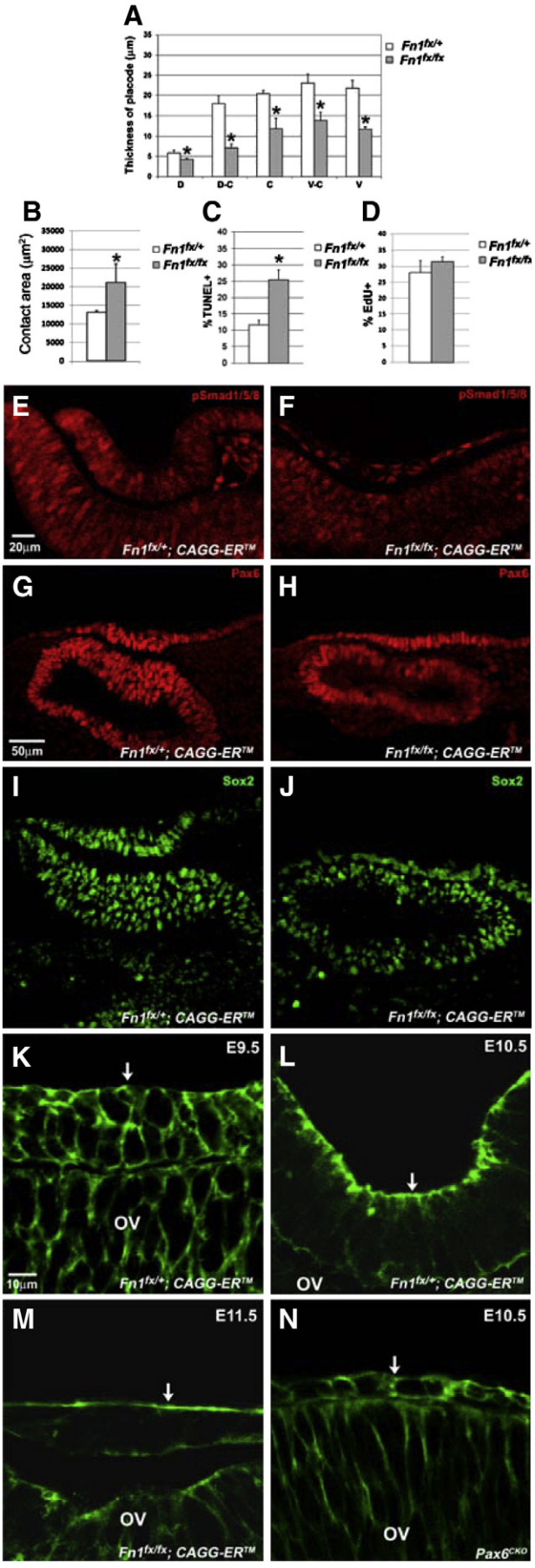

apices, which may drive placode bending to initiate invagination. We stained embryos and cultured heads with phalloidin to determine whether the apical redistribution of the actin cytoskeleton that occurs just prior to invagination occurred in the absence of placode formation. We confirmed that in wild type placodes, F-actin was uniformly distributed around the cell periphery before invagination and localized to the apical ends of the placode cells during invagination (Figs. 5I, J). In *Fn1*-deficient head explants, F-actin also localized to the apical ends of the surface ectoderm cells, although the ectoderm did not invaginate (Fig. 5K). As in placode cells lacking BMP receptors or *Shroom3* (Plageman et al., 2010; Rajagopal et al., 2009), F-actin did not redistribute to the apical ends of cells in the prospective lens-forming ectoderm of $Pax6^{CKO}$ embryos (Fig. 5L).

Discussion

Lens placode formation: a case of matrix-mediated morphogenesis?

Previous investigators demonstrated that restricting the expansion of the embryonic ectoderm resulted in the formation of an epithelial placode. Placing a small metal ring on the ectoderm or ligating the ectoderm with a fine hair caused placode formation (Steding, 1967; Wakely, 1984). Lens placode formation was attributed to restricted expansion of the ectoderm by adhesion to the underlying optic vesicle (Hendrix and Zwaan, 1975; Wakely, 1984; Zwaan and Hendrix, 1973). Zwaan and Hendrix (1973) calculated that the increase in cell number in the fixed area of the placode was sufficient to account for the increase in cell density and cell length seen during placode formation. Based on these observations, Zwaan and co-workers proposed what we have termed the "restricted expansion hypothesis" of lens placode formation: adhesion between the surface ectoderm and the underlying ECM prevents the expansion of the prospective lens ectoderm. Continued cell proliferation within this restricted area results in thickening of the head ectoderm to form the lens placode (Hendrix and Zwaan, 1975; Zwaan and Hendrix, 1973).

As in the chicken embryo, lens placode formation in the mouse embryo was accompanied by an increase in cell density, while the contact area between the optic vesicle and the surface ectoderm did not change. At the same time, the surface area of the ectoderm outside the placode is increasing as a result of the normal growth of the head. During placode formation, the average cell volume and rate of cell proliferation did not change. These data and the results of previous studies on chicken embryos predict that adhesion to the ECM causes

Fig. 5. Treatment of CAGG-ER^{TM} embryos with tamoxifen in vivo followed by culture in tamoxifen prevented placode formation, but did not reduce pSmad1/5/8, Pax6, or Sox2 staining, or the cytoskeletal reorganization that occurs prior to placode invagination. Deletion of *Fn1* decreased placode thickness and increased the contact area between the optic vesicle and the surface ectoderm. (A) Lens placode thickness was significantly decreased in *Fn1*-deficient head explants. (B) The contact area between the ectoderm and the optic vesicle was significantly greater in *Fn1*-deficient head explants. (C) The TUNEL-labeling index increased significantly in *Fn1*-deficient head explants. (D) Cell proliferation, as measured by the EdU-labeling index, was similar in wild type and *Fn1*-deficient head explants. (E, F) BMP signaling, as measured by the nuclear localization of phosphorylated Smad1/5/8 (pSmad1/5/8), occurred in *Fn1*-deficient head explants. (G, H, I, J) Pax6 and Sox2 protein levels were similar in the prospective placodal ectoderm of $Fn1^{fx/+}$and $Fn1^{fx/fx}$ head explants after treatment with tamoxifen. Cytoskeleton reorganization in wild type and $Pax6^{CKO}$ embryos and *Fn1*-deficient head explants (K, L, M, N). (K) Confocal images of phalloidin staining of a frontal section of a $Fn1^{fx/+}$; *CAGG-ER*^{TM} embryo showing the localization of the actin cytoskeleton at the periphery of the lens placode cells on E9.5, before placode invagination. (L) A frontal section of $Fn1^{fx/+}$; *CAGG-ER*^{TM} embryo, showing the mainly apical localization of the F-actin cytoskeleton during placode invagination. (M) Phalloidin staining on a frontal section of a $Fn1^{fx/fx}$; *CAGG-ER*^{TM} head explant that had been cultured in 4-OH tamoxifen, showing the mainly apical localization of the F-actin cytoskeleton at a stage corresponding to the lens vesicle stage in vivo. (N) Phalloidin staining in a frontal section of a $Pax6^{CKO}$ embryo showing the uniform distribution of the F-actin cytoskeleton at the periphery of the surface ectoderm cells at E10.5, when invagination would be occurring in wild type embryos. Arrows point to the apical surface of the ectoderm cells. OV, optic vesicle. *$p<0.05$.

the formation of the lens placode (McKeehan, 1951; Zwaan and Hendrix, 1973) (Fig. 6).

The failure of placode formation after deletion of Pax6 in the prospective lens ectoderm is consistent with the "restricted expansion hypothesis"

Deletion of *Pax6* in the surface ectoderm prevented placode formation and the increase in cell density that occurs during placode formation without altering the BrdU labeling index, cell volume, or decreasing cell death. Importantly, we observed that the contact area between the optic vesicle and the surface ectoderm increased in the $Pax6^{CKO}$ ectoderm. Expansion of the ectoderm and failure of placode formation were accompanied by a substantial decrease in the ECM between the optic vesicle and the ectoderm and a decrease in transcripts encoding components of the ECM. This is the result predicted by the "restricted expansion hypothesis:" if the ECM cannot prevent the ectoderm from expanding, a placode will not form.

Prevention of placode formation by defects in the ECM or reduced adhesion to the ECM is consistent with previous studies on chimeric embryos containing $Pax6^{+/+}$ and $Pax6^{-/-}$ cells, which showed that most $Pax6^{-/-}$ cells were eliminated from the lens placode (Collinson et al., 2000). Presumably, this occurred because the $Pax6^{-/-}$ cells had decreased adhesion to the underlying matrix and were excluded by the more adhesive $Pax6^{+/+}$ cells. This study also showed that contact between the optic vesicle and the ectoderm was not robust when either or both epithelia had a high proportion of $Pax6^{-/-}$ cells. These data suggest that cells lacking *Pax6* have lower adhesion to the ECM. This could be due to defects in the ECM produced by $Pax6^{-/-}$ cells, defects in the adhesion of $Pax6^{-/-}$ cells to the matrix, or both.

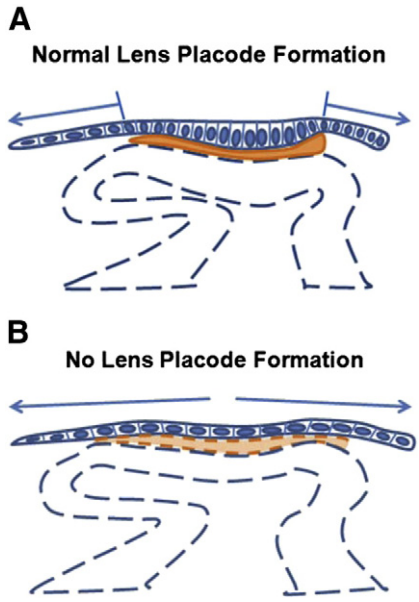

Fig. 6. The "restricted expansion hypothesis" of lens placode formation. The extracellular matrix between the optic vesicle and the surface ectoderm is colored orange. (A) During normal lens placode formation, the adhesion between the head ectoderm and the extracellular matrix prevents the expansion of the prospective lens territory. Continued cell proliferation within this area of adhesion leads to cell crowding, resulting in cell elongation and placode formation (Hendrix and Zwaan, 1975). The arrows indicate that the head ectoderm outside the placode continues to expand as the embryos grows (B) In $Pax6^{CKO}$ and *Fn1*-deficient embryos, the matrix between the optic vesicle and the overlying head ectoderm is deficient, resulting in the unrestricted expansion of the prospective lens ectoderm (arrows) and impaired placode formation.

Global deletion of Fn1 permitted expansion of the ectoderm and prevented placode formation

To further test the "restricted expansion hypothesis" we disrupted the assembly and function of the ECM by deleting *Fn1*. Fibronectin is required for the assembly of the ECM and for cell–matrix adhesion (Akiyama et al., 1989; Corbett et al., 1997; Huang et al., 2007; Leiss et al., 2008; Mattey and Garrod, 1984; Oberley and Steinert, 1983; Wierzbicka-Patynowski and Schwarzbauer, 2003). Fibronectin binds to cell-surface integrins, which promotes the assembly of a fibrillar fibronectin matrix. The fibronectin matrix then acts as a template for the assembly other components of the ECM (Leiss et al., 2008). We reasoned that insufficient levels of fibronectin might disrupt the assembly of a functional matrix between the optic vesicle and surface ectoderm. If the restricted expansion hypothesis is correct, failure of proper matrix assembly and function should prevent placode formation.

Deletion of *Fn1* using ubiquitously-expressed, tamoxifen-inducible Cre recombinase reduced fibronectin in the ECM between the optic vesicle and the surface ectoderm and prevented the formation of a lens placode and placode invagination. As in the $Pax6^{CKO}$ ectoderm, the area of contact between the optic vesicle and the surface ectoderm expanded in $Fn1^{CKO}$ embryos compared to embryos heterozygous for *Fn1*. These results were consistent with the key predictions of the "restricted expansion hypothesis:" adhesion to intact ECM restricts the expansion of the ectoderm and spreading of the ectoderm prevents placode formation.

Differences between deletion of Pax6 and Fn1 in the surface ectoderm

Removal of one *Pax6* allele with the Le-Cre transgene reduced the thickness of the lens placode, but did not prevent lens invagination. Loss of both *Pax6* alleles from the ectoderm prevented placode formation and invagination. However, presumed deletion of *Fn1* from the lens placode using the same Le-Cre transgene did not inhibit placode formation or prevent invagination. Therefore, other *Pax6* target genes must contribute to placode formation. These may include genes encoding other components of the ECM that are reduced in $Pax6^{CKO}$ placodes (Table 1), or genes required to maintain the adhesion of placode cells with the ECM. Further studies are required to identify the *Pax6*-regulated genes that are required in the ectoderm for placode formation.

We observed that fibronectin protein persisted between the ectoderm and the optic vesicle after the presumed deletion of *Fn1* from the ectoderm using the Le-Cre transgene, from the optic vesicle using the Rx-Cre transgene, or both. However, extracellular fibronectin persisted after deletion of *Fn1*, presumably restricting expansion of the ectoderm. This view was supported by deletion of *Fn1* at an earlier stage, using a ubiquitously-expressed, tamoxifen-inducible transgene, which significantly reduced the accumulation of fibronectin beneath the ectoderm, permitted the ectoderm to expand and prevented lens placode formation.

Why make a placode?

Placodes form prior to the invagination of many tissues, but an explanation of why this occurs has not been provided and, to our knowledge, the requirement of placode formation for subsequent invagination has not been tested. Just before the invagination of the lens placode, actin filaments decrease at the lateral surfaces of the placode cells and increase at their apical ends. This cytoskeletal reorganization requires Pax6, BMP signaling and the scaffold protein, Shroom3 (Plageman et al., 2010; Rajagopal et al., 2009). Deletion of *Pax6* from the prospective lens ectoderm or *Fn1* from the entire embryo prevented placode formation. However, unlike deletion of *Pax6*, loss of fibronectin from the lens ECM did not prevent the apical

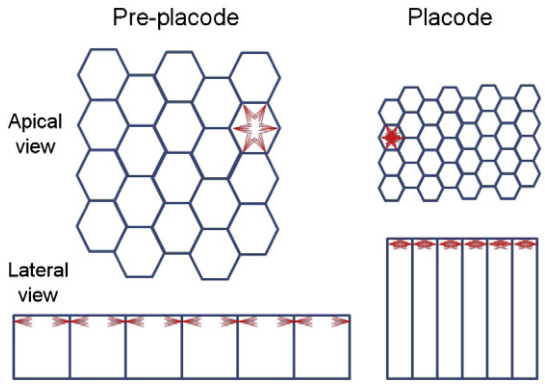

Fig. 7. Illustration of the geometric consequences of doubling cell height while maintaining cell volume. During lens placode formation, crowding causes cell elongation, resulting in a fourfold decrease in the area of the apical end of each cell and a fourfold increase in the "concentration" of cell apices. If the concentration of apical actin filaments (red lines) were similar on a per-cell basis, the concentration of these filaments at the apical end of each cell would be at least four times higher after placode formation, resulting in a sixteen-fold increase in their concentration at the apical surface. Actin filaments are depicted as red lines of equal length and number in each tissue.

localization of the actin cytoskeleton. Thus, it appears that, after deletion of *Fn1*, the lens-forming ectoderm cells are prepared for invagination, but invagination fails. These observations are consistent with the possibility that placode formation is a mechanical precondition for invagination.

From a mechanical perspective, the formation of a placode would seem to make its deformation (invagination) more difficult, since more force is required to bend a thicker tissue. However, if the contractile apparatus assembled at the apical ends of each placode cell provides the force required to bend the placode during invagination, having a larger number of longer, thinner cells could decrease the force required from each cell to bend the tissue (Fig. 7). Doubling the length of a cell while maintaining its volume, as occurs during lens placode formation, increases the number of cell apices per area by a factor of four. This process also decreases by a factor of four the average area of the apical ends of the placode cells. Together with the apical localization of actin filaments that occurs prior to invagination (Plageman et al., 2010; Rajagopal et al., 2009), reducing the apical area of the cells would increase the density of actin filaments in the apical actin web (Fig. 7). Since actin filaments of opposite polarity interact with myosin II to promote contraction (Ivanov, 2008; Plageman et al., 2010), increasing the density of actin filaments could increase the interaction between actin filaments and myosin II. Together, these changes should increase the force available to reduce the apical surface area of the tissue and drive invagination.

Conclusions

The studies presented test the main prediction of the "restricted expansion hypothesis" of lens placode formation. They suggest that the integrity of the ECM between the optic vesicle and the lens is necessary for lens placode formation. When the matrix was disrupted and/or cell–matrix interactions were decreased, the ectoderm spread and the lens placode did not form. Our data also suggest that placode formation is required to establish the mechanical conditions necessary for invagination of the lens placode to form the lens pit. If confirmed, this could explain why placode formation precedes epithelial invagination throughout development.

Acknowledgments

The authors thank Anand Swaroop, Eric Swindell and Milan Jamrich for providing the Rx-Cre mice and Reinhard Fässler and Erkki Ruoslahti for the *Fn1* floxed mice. The Pax6 monoclonal antibody developed by A. Kawakami was obtained from the Developmental Studies Hybridoma Bank developed under the auspices of the NICHD and maintained by The University of Iowa, Department of Biology, Iowa City, IA 52242. We thank Belinda McMahan and Jean Jones for excellent histological support. Research was supported by NIH grant EY04853 (DCB), NIH core grant EY02687 to the Department of Ophthalmology and Visual Sciences (DOVS), and an unrestricted grant from Research to Prevent Blindness to the DOVS.

Appendix A. Supplementary data

Supplementary data to this article can be found online at doi:10.1016/j.ydbio.2011.04.008.

References

Akiyama, S.K., Yamada, S.S., Chen, W.T., Yamada, K.M., 1989. Analysis of fibronectin receptor function with monoclonal antibodies: roles in cell adhesion, migration, matrix assembly, and cytoskeletal organization. J. Cell Biol. 109, 863–875.
Allen, B.L., Rapraeger, A.C., 2003. Spatial and temporal expression of heparan sulfate in mouse development regulates FGF and FGF receptor assembly. J. Cell Biol. 163, 637–648.
Almeida, E.A., Ilic, D., Han, Q., Hauck, C.R., Jin, F., Kawakatsu, H., Schlaepfer, D.D., Damsky, C.H., 2000. Matrix survival signaling: from fibronectin via focal adhesion kinase to c-Jun NH(2)-terminal kinase. J. Cell Biol. 149, 741–754.
Ashery-Padan, R., Marquardt, T., Zhou, X., Gruss, P., 2000. Pax6 activity in the lens primordium is required for lens formation and for correct placement of a single retina in the eye. Genes Dev. 14, 2701–2711.
Collinson, J.M., Hill, R.E., West, J.D., 2000. Different roles for Pax6 in the optic vesicle and facial epithelium mediate early morphogenesis of the murine eye. Development 127, 945–956.
Corbett, S.A., Lee, L., Wilson, C.L., Schwarzbauer, J.E., 1997. Covalent cross-linking of fibronectin to fibrin is required for maximal cell adhesion to a fibronectin-fibrin matrix. J. Biol. Chem. 272, 24999–25005.
Cvekl, A., Duncan, M.K., 2007. Genetic and epigenetic mechanisms of gene regulation during lens development. Prog. Retin. Eye Res. 26, 555–597.
Danen, E.H., Yamada, K.M., 2001. Fibronectin, integrins, and growth control. J. Cell. Physiol. 189, 1–13.
Furuta, Y., Hogan, B.L., 1998. BMP4 is essential for lens induction in the mouse embryo. Genes Dev. 12, 3764–3775.
Garcia, C.M., Huang, J., Madakashira, B.P., Liu, Y., Rajagopal, R., Dattilo, L., Robinson, M.L., Beebe, D.C., 2011. The function of FGF signaling in the lens placode. Dev. Biol. 351, 176–185.
George, E.L., Georges-Labouesse, E.N., Patel-King, R.S., Rayburn, H., Hynes, R.O., 1993. Defects in mesoderm, neural tube and vascular development in mouse embryos lacking fibronectin. Development 119, 1079–1091.
Gregory, K.E., Ono, R.N., Charbonneau, N.L., Kuo, C.L., Keene, D.R., Bachinger, H.P., Sakai, L.Y., 2005. The prodomain of BMP-7 targets the BMP-7 complex to the extracellular matrix. J. Biol. Chem. 280, 27970–27980.
Gundersen, H.J., Bendtsen, T.F., Korbo, L., Marcussen, N., Moller, A., Nielsen, K., Nyengaard, J.R., Pakkenberg, B., Sorensen, F.B., Vesterby, A., et al., 1988. Some new, simple and efficient stereological methods and their use in pathological research and diagnosis. APMIS 96, 379–394.
Hayashi, S., McMahon, A.P., 2002. Efficient recombination in diverse tissues by a tamoxifen-inducible form of Cre: a tool for temporally regulated gene activation/inactivation in the mouse. Dev. Biol. 244, 305–318.
Hendrix, R.W., Zwaan, J., 1974. Changes in the glycoprotein concentration of the extracellular matrix between lens and optic vesicle associated with early lens differentiation. Differentiation 2, 357–362.
Hendrix, R.W., Zwaan, J., 1975. The matrix of the optic vesicle-presumptive lens interface during induction of the lens in the chicken embryo. J. Embryol. Exp. Morphol. 33, 1023–1049.
Huang, S.D., Liu, X.H., Bai, C.G., Lu, F.L., Yuan, Y., Gong, D.J., Xu, Z.Y., 2007. Synergistic effect of fibronectin and hepatocyte growth factor on stable cell–matrix adhesion, re-endothelialization, and reconstitution in developing tissue-engineered heart valves. Heart Vessels 22, 116–122.
Ivanov, A.I., 2008. Actin motors that drive formation and disassembly of epithelial apical junctions. Front. Biosci. 13, 6662–6681.
Lang, R.A., 2004. Pathways regulating lens induction in the mouse. Int. J. Dev. Biol. 48, 783–791.
Leiss, M., Beckmann, K., Girós, A., Costell, M., Fässler, R., 2008. The role of integrin binding sites in fibronectin matrix assembly in vivo. Curr. Opin. Cell Biol. 20, 502–507.
Mattey, D.L., Garrod, D.R., 1984. Organization of extracellular matrix by chick embryonic corneal epithelial cells in culture and the role of fibronectin in adhesion. J. Cell Sci. 67, 171–188.
McKeehan, M.S., 1951. Cytological aspects of embryonic lens induction in the chick. J. Exp. Zool. 117, 31–64.
Naiche, L.A., Papaioannou, V.E., 2007. Cre activity causes widespread apoptosis and lethal anemia during embryonic development. Genesis 45, 768–775.

Oberley, T.D., Steinert, B.W., 1983. Effect of the extracellular matrix molecules fibronectin and laminin on the adhesion and growth of primary renal cortical epithelial cells. Virchows Arch. B Cell Pathol. Incl. Mol. Pathol. 44, 337–354.
Pan, Y., Carbe, C., Powers, A., Zhang, E.E., Esko, J.D., Grobe, K., Feng, G.S., Zhang, X., 2008. Bud specific N-sulfation of heparan sulfate regulates Shp2-dependent FGF signaling during lacrimal gland induction. Development 135, 301–310.
Plageman Jr., T.F., Chung, M.I., Lou, M., Smith, A.N., Hildebrand, J.D., Wallingford, J.B., Lang, R.A., 2010. Pax6-dependent Shroom3 expression regulates apical constriction during lens placode invagination. Development 137, 405–415.
Rajagopal, R., Huang, J., Dattilo, L.K., Kaartinen, V., Mishina, Y., Deng, C.X., Umans, L., Zwijsen, A., Roberts, A.B., Beebe, D.C., 2009. The type I BMP receptors, Bmpr1a and Acvr1, activate multiple signaling pathways to regulate lens formation. Dev. Biol. 335, 305–316.
Reza, H.M., Ogino, H., Yasuda, K., 2002. L-Maf, a downstream target of Pax6, is essential for chick lens development. Mech. Dev. 116, 61–73.
Sakai, T., Johnson, K.J., Murozono, M., Sakai, K., Magnuson, M.A., Wieloch, T., Cronberg, T., Isshiki, A., Erickson, H.P., Fassler, R., 2001. Plasma fibronectin supports neuronal survival and reduces brain injury following transient focal cerebral ischemia but is not essential for skin-wound healing and hemostasis. Nat. Med. 7, 324–330.
Seib, F.P., Lanfer, B., Bornhauser, M., Werner, C., 2010. Biological activity of extracellular matrix-associated BMP-2. J. Tissue Eng. Regen. Med. 4 (4), 324–327.
Smith, S.M., West, L.A., Govindraj, P., Zhang, X., Ornitz, D.M., Hassell, J.R., 2007. Heparan and chondroitin sulfate on growth plate perlecan mediate binding and delivery of FGF-2 to FGF receptors. Matrix Biol. 26, 175–184.
Smith, A.N., Miller, L.-A., Radice, G., Ashery-Padan, R., Lang, R.A., 2009. Stage-dependent modes of Pax6-Sox2 epistasis regulate lens development and eye morphogenesis. Development 136, 2977–2985.
Steding, G., 1967. Reasons for embryonic epithelial thickening. Acta Anat. 68, 37–67.
Swindell, E.C., Bailey, T.J., Loosli, F., Liu, C., Amaya-Manzanares, F., Mahon, K.A., Wittbrodt, J., Jamrich, M., 2006. Rx-Cre, a tool for inactivation of gene expression in the developing retina. Genesis 44, 361–363.
Wakely, J., 1984. Observations on the role of ectodermal spreading in the early stages of lens placode invagination in the chick embryo. Exp. Eye Res. 38, 627–636.
Wierzbicka-Patynowski, I., Schwarzbauer, J.E., 2003. The ins and outs of fibronectin matrix assembly. J. Cell Sci. 116, 3269–3276.
Zhu, Y., Oganesian, A., Keene, D.R., Sandell, L.J., 1999. Type IIA procollagen containing the cysteine-rich amino propeptide is deposited in the extracellular matrix of prechondrogenic tissue and binds to TGF-beta1 and BMP-2. J. Cell Biol. 144, 1069–1080.
Zwaan, J., Hendrix, R.W., 1973. Changes in cell and organ shape during early development of the ocular lens. Amer. Zool. 13, 1039–1049.
Zwaan, J., Pearce, T.L., 1971. Cell population kinetics in the chicken lens primordium during and shortly after its contact wth the optic cup. Dev. Biol. 25, 96–118.
Zwaan, J., Webster, E.H., 1984. Histochemical analysis of extracellular matrix material during embryonic mouse lens morphogenesis in an aphakic strain of mice. Dev. Biol. 104, 380–389.